

# Interactional aerodynamics and acoustics of a hingeless coaxial helicopter with an auxiliary propeller in forward flight

H. W. Kim

hkim@eng.gla.ac.uk

Department of Aeronautics  
Imperial College London  
London, UK

A. R. Kenyon

adam.kenyon04@imperial.ac.uk

R. E. Brown

rbrown@aero.gla.ac.uk

Department of Aerospace Engineering  
University of Glasgow  
Glasgow, UK

K. Duraisamy

dkarthik@aero.gla.ac.uk

## ABSTRACT

The aerodynamics and acoustics of a generic coaxial helicopter with a stiff main rotor system and a tail-mounted propulsor are investigated using Brown's Vorticity Transport Model. In particular, the model is used to capture the aerodynamic interactions that arise between the various components of the configuration. By comparing the aerodynamics of the full configuration of the helicopter to the aerodynamics of various combinations of its sub-components, the influence of these aerodynamic interactions on the behaviour of the system can be isolated. Many of the interactions follow a simple relationship between cause and effect. For instance, ingestion of the main rotor wake produces a direct effect on the unsteadiness in the thrust produced by the propulsor. The causal relationship for other interdependencies within the system is found to be more obscure. For instance, a dependence of the acoustic signature of the aircraft on the tailplane design originates in the changes in loading on the main rotor that arise from the requirement to trim the load on the tailplane that is induced by its interaction with the main rotor wake. The traditional approach to the analysis of interactional effects on the performance of the helicopter relies on characterising the system in terms of a network of possible interactions between the separate components of its configuration. This approach, although conceptually appealing, may obscure the closed-loop nature of some of the aerodynamic interactions within the helicopter system. It is suggested that modern numerical simulation techniques may be ready to supplant any overt reliance on this reductionist type approach and hence may help to forestall future repetition of the long history of unforeseen, interaction-induced dynamic problems that have arisen in various new helicopter designs.

## NOMENCLATURE

$C_D$	fuselage drag coefficient
$C_F$	rotor force coefficient
$C_M$	rotor moment coefficient
$C_P$	rotor power coefficient
$C_T$	rotor thrust coefficient
$C_X$	propulsor force coefficient
$C_W$	helicopter weight coefficient
$F$	vector of overall forces and moments
$l$	fuselage half-length
$N_b$	number of blades
$R$	rotor radius
$v_i$	induced velocity
$\mu$	advance ratio
$\psi$	blade azimuth
$\Omega$	rotor rotational speed

## Subscripts/superscripts

$c$	coaxial system
$t$	propulsor
$x, y, z$	orthogonal Cartesian components
*	trim target

**Important note:** throughout this paper, the upper rotor of the coaxial system should be taken to rotate anticlockwise, and the lower rotor to rotate clockwise, when viewed from above.

## 1.0 INTRODUCTION

Recent design studies have revisited the twin contra-rotating coaxial rotor system as a potential solution to the emerging requirement for a heavy-lift helicopter that can achieve much higher forward speed than has traditionally been possible with single-rotor platforms<sup>(1)</sup>.

With a conventional single rotor system with an articulated hub (or a hingeless hub but with low flapwise stiffness) the maximum performance of the system in forward flight is often limited by the high lift coefficients that are required on the retreating side of the rotor disc in order to overcome the natural tendency of the rotor to flap backwards. The same limitation applies to conventional coaxial rotors where the hubs of the individual rotors are articulated. Unique to a coaxial configuration, though, is the prospect of introducing significant flapwise stiffness into the system in order to relieve the retreating blade from the requirement to operate at high lift coefficients. The presence of flapwise stiffness alters the phase relationship between blade flapping and the applied aerodynamic load such that the natural response of a stiffened rotor in forward flight is no longer to flap backwards but instead to produce a rolling moment about its hub. The contributions to the rolling moment from two contra-rotating rotors can be made to cancel naturally, however, and this allows the retreating sides of the rotors to be flown at relatively benign average lift coefficients compared to those associated with a conventional rotor. As a result, such rotors can be flown at much higher advance ratios than traditional single main rotor systems before the aerodynamics of the retreating blades pose a serious limit to the performance of the system. This is essentially the design philosophy of the Advancing Blade Concept (ABC) rotor system developed by Sikorsky Aircraft Corporation and implemented on the prototype XH-59A aircraft in the 1970s (see Refs 2 and 3 for a detailed overview of the development of this helicopter).

At high forward speed, the effects of compressibility at the tip of the advancing blade pose a limit on the performance of the rotor regardless of the flapwise stiffness of the system. The effects of compressibility can be delayed to higher forward speed however if the main rotor system can be off-loaded by a suitable means of lift or thrust augmentation, thus allowing for reduced rotational speed of the main rotor<sup>(4)</sup>. The XH-59A itself used a pair of turbojets to augment the thrust produced by the main rotor. This design did not reach production, but, aided by recent advancements in composite material technology and vibration suppression techniques, Sikorsky has revived the stiffened coaxial rotor concept in the development of its X2 technology demonstrator (see Fig. 1 taken from Ref. 1).

The prototype X2 uses a tail-mounted pusher propeller to augment the propulsive force that is provided by its ABC-type coaxial rotor. The interactional aerodynamics associated with a compound helicopter with such a configuration have recently been investigated by Kim *et al* using Brown's Vorticity Transport Model<sup>(5)</sup>. Since the earliest days of rotary-winged flight, prototype helicopters have been plagued by the effects of

unforeseen aerodynamic interactions between their various components. The principal motivation for Kim *et al*'s study was to provide evidence to counter the long-held belief that the aerodynamic behaviour of rotorcraft is largely not amenable to reliable computation – at least down to the detail required to resolve these interactions accurately enough for reliable preventive design measures to be taken.

The fictitious aircraft analysed in Kim *et al*'s study was similar to the Sikorsky concept in that it consisted of a stiff coaxial rotor system, mounted above a compact but streamlined fuselage with a rear-mounted tailplane to provide pitch stability. Thrust augmentation was provided by a rear-mounted propeller, or 'propulsor', mounted in a pusher configuration. The performance of the system in steady level flight at various forward speeds was evaluated and a number of strong aerodynamic interactions between the lifting components of the vehicle were identified. Although many of the interactions could quite feasibly have been ameliorated by fairly straightforward design modifications to the configuration, some of the interactions would have had significant impact on the dynamics and performance of the system. For example, the main rotor wake was shown to induce a large download on the tailplane that resulted in a nose-up pitching moment at low advance ratio. This moment resulted in an increase in the loading on the rear of the main rotor in order to maintain the vehicle in trim. The highly loaded region at the rear of the rotor discs resulted in an unexpected concentration, immediately below the rear edge of the main rotor, of the noise produced by blade vortex interactions. Similarly, at low forward speed, the thrust produced by the propulsor was found to be highly unsteady. The cause of this unsteadiness was traced to the aerodynamic effects of ingestion through the propulsor disc of vortical structures produced by the main rotor.

These examples and others like them were used in Kim *et al*'s study to argue that the state of the art in computational modelling of helicopter aerodynamics has advanced to a stage where detailed insight into the interactive aerodynamic environment of a new rotorcraft, even one with as complex a configuration as that of the compounded coaxial helicopter, can indeed be obtained early in its development and possibly even integrated into its design.

The present paper aims to investigate further the origins of the aerodynamic characteristics of the helicopter configuration that was studied by Kim *et al*. In particular, this paper aims to shed light on how the performance of the sub-components of the system in isolation are modified by aerodynamic interaction with the other sub-components of the system once integrated into the configuration of the helicopter. In this vein, the aerodynamic characteristics of several different combinations of the main rotor system, fuselage, and propulsor are contrasted in order to reveal the processes through which their aerodynamic interaction influences the aerodynamic and acoustic character of the overall helicopter system.



Figure 1. Sikorsky's X2 technology demonstrator. (Courtesy of Ashish Bagai, Sikorsky Aircraft Corporation.)

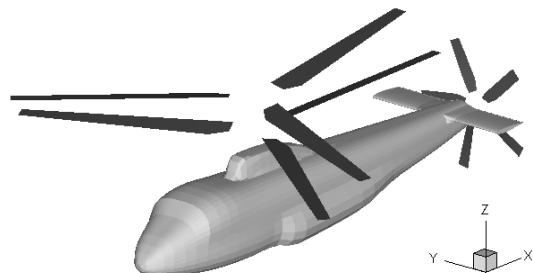


Figure 2. Generic thrust-compounded hingeless coaxial configuration.

**Table 1**  
Main rotor and propulsor geometries

Rotor radius	Main Rotor $R_c$ (5.5m)	Propulsor $R_t$ (0.28 $R_c$ )
Number of rotors	2	1
Blades per rotor	3	5
Rotor separation	0.139 $R_c$	–
Root cutout	0.12 $R_c$	0.20 $R_t$
Solidity	0.127	0.222
Twist	–10.0°	–30.0°
Chord	Tapered (2:1)	0.18 $R_t$
Aerofoil sections	NACA 23012	NACA 0012

## 2.0 COMPUTATIONAL MODEL

The Vorticity Transport Model (VTM) developed by Brown<sup>(6)</sup> and extended by Brown and Line<sup>(7)</sup> is used in this paper to simulate the aerodynamics of a generic, thrust-compounded coaxial helicopter and its components. The VTM provides an Eulerian representation of the dynamics of the vorticity in the wake of the vehicle by advancing the unsteady Navier-Stokes equations, written in vorticity-velocity form, through time on a structured Cartesian mesh enclosing the rotorcraft. The use of an adaptive grid system in a semi-Lagrangian manner to track the evolution of the vorticity field enhances the computational efficiency of the method. The overall cell count is reduced by using a sequence of nested grids in which increasingly coarser cells are arranged with increasing distance from the rotor. An extension of the Weissinger-L version of lifting-line theory is used, in conjunction with a look-up table for the two-dimensional aerodynamic characteristics of the rotor blade sections, to represent the blade aerodynamics. The fuselage aerodynamics are modelled using a vortex panel approach in which the condition of zero through-flow is satisfied at the centroid of each panel. Lift generation by the fuselage is modelled by applying the Kutta condition along pre-specified separation lines on its surface. The viscous wake of the fuselage is not accounted for, however. The reader is referred to Refs 5 and 8 for a more detailed account of the application of the VTM to the modelling of entire helicopter configurations.

In terms of verification of this approach, the VTM has been used to investigate the aerodynamic behaviour of isolated coaxial rotors<sup>(9)</sup> and has been shown to capture accurately the performance of such systems. The fuselage model coupled with the VTM has also been used successfully to investigate the aerodynamic interactions experienced by the NASA ROBIN helicopter configuration, and the model has been shown to produce very good agreement with experimental results for the mean and time-dependent variation of inflow through the rotor, the position of the wake vortices as they approach the surface of the fuselage, and both the mean and time-variation of the pressure fields that are induced on the surface of the fuselage by these vortical structures<sup>(8)</sup>. These previous studies provide some confidence that the model is able to capture those features of the aerodynamic environment of the vehicle that are of most relevance to the present study.

In the present context, the VTM is particularly well suited to resolving the wake-induced interactions between geometrically well-separated components of the aircraft. The convection algorithm implemented in the VTM is particularly effective in controlling the local rate of numerical dissipation of vorticity, thus maintaining the integrity of vortical structures in the rotor wake for the many rotor revolutions required to capture the aerodynamic interactions between even the furthest-separated components of the helicopter. This property of the model enables the long-range aerodynamic interactions between the twin main rotors, the tail propulsor and the horizontal stabiliser of the generic helicopter configuration studied in this paper to be analysed in detail.

**Table 2**  
Fuselage geometry

Fuselage length (2l)	2.04 $R_c$
Tailplane:	
Aerofoil section	NACA 0012
Span	0.667l
Chord	0.167l
Hub x,y,z co-ordinates:	
rotor (lower)	0.765l, 0.000l, 0.386l
Main rotor (upper)	0.765l, 0.000l, 0.522l
Propulsor	2.079l, 0.000l, 0.111l
(relative to fuselage nose)	

## 3.0 MODEL DESCRIPTION

The generic helicopter configuration studied in this paper consists of a stiffened contra-rotating coaxial rotor system together with a tail-mounted auxiliary propulsor to augment the propulsive component of the thrust that is produced by the main rotor system (see Fig. 2). Each of the components of this configuration is described in detail below, but a more complete geometric description can be found in Ref. 5.

### 3.1 Rotor system

The main rotor of the modelled system consists of twin contra-rotating, three-bladed rotors with a vertical separation of 0.139 $R_c$ . The blades of both rotors have 2:1 linear taper and 10° of non-linear twist. A single aerofoil section, NACA 23012, is used along the entire span of the rotor blades. In reality, the blades of ABC-type rotors feature a rather more complex spanwise variation of aerofoil section and twist than that modelled here<sup>(1,10)</sup>. Nevertheless the broad characteristics of the wake produced by the main rotor, and hence the aerodynamic interference between the main rotor system and the other components of the simplified configuration modelled here should be sufficiently representative of a realistic full-scale vehicle of this type. The geometric properties of the main rotor system are summarised in Table 1.

The flapwise stiffness of the ABC-type rotors modelled in this study is approximated, somewhat crudely, by assuming the rotor blades and their attachments to the rotor hub to be completely rigid. The loading on the rotors and the resulting wake geometry of a completely rigid coaxial rotor system has been shown to be very similar<sup>(11)</sup> to that of rotors with the high level of flapwise stiffness that is characteristic of the coaxial rotors of ABC-type systems<sup>(12,13)</sup>, however. Thus, as far as the effects of aerodynamic interference are concerned, the simplified rigid rotor model is expected to provide a realistic representation of the aerodynamic environment that is generated by practical semi-rigid coaxial rotor systems.

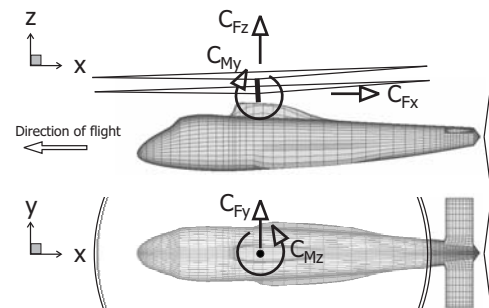


Figure 3. Schematic showing the axis convention for forces and moments.

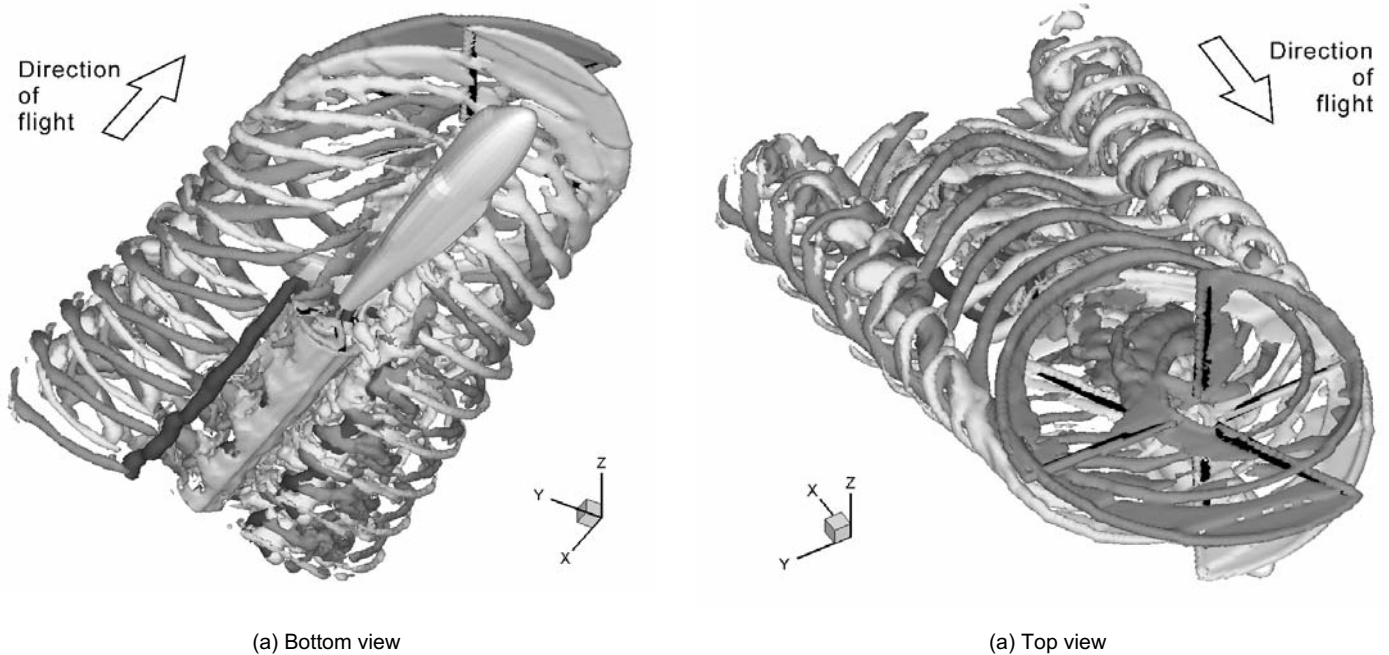


Figure 4. Visualisation of the wake structure of the full configuration in steady forward flight at advance ratio  $\mu = 0.15$ . (Wakes from the different elements of the configuration coloured in separate shades of grey)

### 3.2 Auxiliary propulsor

The auxiliary device used to augment the propulsive thrust component produced by the main rotor consists of a five-bladed propeller mounted in a pusher configuration at the rear of the fuselage. This propulsor is oriented such that its rotational axis is aligned with the longitudinal axis of the aircraft. Each blade has a rectangular planform, a constant NACA 0012 sectional profile and  $30^\circ$  of linear twist. The radius of the propulsor is  $0.28R_c$  and the rotational speed is fixed at 4.25 times that of the main rotor. The tip speed of the propulsor is thus 19% greater than that of the main rotor.

The pitch angle of all the blades of the propulsor is adjusted collectively to produce the desired level of thrust. The blades of the propulsor and their attachments to their hub are otherwise assumed to be rigid<sup>†</sup>. The geometry of the propulsor is summarised in Table 1.

### 3.3 Fuselage geometry

The geometry of the fuselage used in the study is entirely fictitious but was chosen to be representative of the compact but streamlined configuration of modern high-performance helicopters (see Fig. 2). The aerodynamic interaction between the wake from the main rotor and the empennage has been documented as being responsible for a number of unexpected flight mechanic issues in modern helicopters (see, for example, Refs 14–19). To allow this source of aerodynamic interaction to be explored, a large horizontal tailplane is mounted at the top of the rear fuselage to represent current design practice. The tailplane is rectangular in planform and has a NACA 0012 sectional profile. The Kutta condition is satisfied along its entire trailing edge thus allowing it to act as a lifting surface. The geometric properties of the fuselage are summarised in Table 2.

### 3.4 Flight condition and trim

In Ref. 5, the aerodynamic performance of the configuration described above was analysed at various forward flight speeds, and the various aerodynamic interactions that manifested at different

advance ratios were described in detail. Of the various forward speeds simulated in this earlier study, the broadest and most interesting range of interactions between the various components of the system were encountered at the relatively moderate advance ratio of  $\mu = 0.15$ . The present paper concentrates solely on the aerodynamic interference between the various components of the compounded hingeless coaxial helicopter at this forward flight speed, and attempts to analyse in detail the influence of each component on the aerodynamic characteristics of the remainder of the configuration.

The self-induced aerodynamic environment of the helicopter is strongly influenced by the method that is used to trim the rotorcraft. The compounded coaxial configuration in particular has several redundant degrees of freedom that can be used in various ways to produce overall force and moment balance within the system. For this reason, the method used to trim the simulated vehicle is set out in detail below.

Given the xyz-co-ordinate system shown in Fig. 3, the array

$$F = [C_{Fx}, C_{Fy}, C_{Fz}, C_{Mx}, C_{My}, C_{Mz}] \quad \dots (1)$$

contains the Cartesian components of the overall forces and moments that are applied by the rotor system and the other lifting components to some suitable reference point on the airframe. For present purposes, the system is assumed to be in trim when the net moment about the base of the main rotor mast is zero, and the propulsive force and the vertical component of the force produced by the system are balanced by the drag and the weight of the aircraft respectively. This trim state of the system is thus defined by the array of prescribed target loads on the vehicle

$$F^* = [-C_D, 0, C_W, 0, 0, 0] \quad \dots (2)$$

In all simulations the weight of the aircraft was fixed at  $C_W = 0.012$ , and the drag of the system was calculated as  $C_D = 0.00072$  at  $\mu = 0.15$  by assuming the parasite drag of the system to be represented by an equivalent flat plate<sup>(20)</sup> with  $1/25^{\text{th}}$  of the main rotor disc area. These values are roughly representative of an aircraft of the size of the XH-59A<sup>(21)</sup>.

<sup>†</sup> Note that, as with the main rotor system, the hub of the propulsor is not modelled for further simplicity.

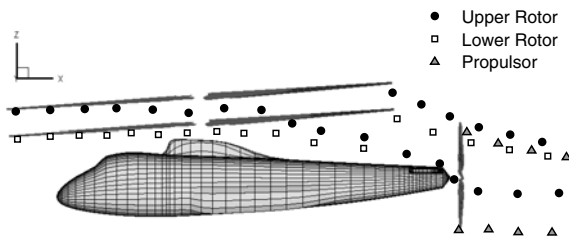


Figure 5. Trajectories of the tip vortices of the main rotors and propulsor at advance ratio  $\mu = 0.15$  showing the points of intersection of individual vortices with the longitudinal plane through the fuselage centreline.

To trim the aircraft, the system is driven into a condition such that  $\bar{F} = F^*$ , where  $\bar{F}$  is the long-term average of  $F(t)$ , by suitable control input. In all simulations presented in this paper, the collective pitch inputs to both upper and lower rotors are varied together to alter the total thrust produced by the system while differential collective pitch input to the upper and lower rotors is used to maintain zero net yawing moment on the system. The XH-59A employed differential cyclic pitch input to optimise the performance of the rotor<sup>(2,13,22,23)</sup>, but in the present analysis this feature of the ABC system is ignored and the same cyclic pitch inputs are applied simultaneously to both upper and lower rotors to generate the required rolling and pitching moments on the system. The rigidity of the main rotor system limits the ability of the cyclic pitch controls to tilt the tip path plane relative to the rotor shaft in order to produce a propulsive thrust component to the system, but the high control power of the stiffened rotors allows very direct control of the pitch attitude of the aircraft and hence the disc tilt with respect to the flightpath. The balance of propulsive force between the main rotor system and propulsor that is required to maintain a given forward flight speed is thus largely controlled by the pitch moment that is demanded from the main rotor system. For the simulations presented here, sufficient pitching moment was demanded from the main rotor to cause its tip path plane to incline  $4^\circ$  forward, thereby allowing the main rotor to contribute partially to the forward component of thrust that is required to maintain the forward speed of the helicopter. Any deficit in the propulsive force that is generated by the main rotor is then provided by the tail propulsor by suitable variation of its own collective pitch.

To allow valid comparison between the performance of the entire configuration and that of its various components in isolation, and hence to expose the effects of aerodynamic interaction on the performance of the system, care must be taken to match as closely as possible the operating conditions of the various systems being compared. Calculations of the performance of the rotor system with the fuselage absent were thus conducted with the rotor system trimmed to the same overall conditions on weight, drag and moment as for the full configuration. Calculations of the performance of the isolated propulsor were conducted with this device trimmed to produce the same propulsive thrust as when integrated into the full configuration.

#### 4.0 INTERACTIONAL AERODYNAMICS

Figure 4 shows snapshots, from two perspectives, of the wake structure that is generated by the full helicopter configuration at an advance ratio of  $\mu = 0.15$ . In this figure, a set of iso-surfaces, on which the magnitude of the vorticity in the flow around the vehicle is constant, are presented in various shades of grey to distinguish the wakes that are generated by each of the main rotors, the tail propulsor and the horizontal tail surface. To aid in the interpretation of these figures, Fig. 5 reveals the relative extent of the wake

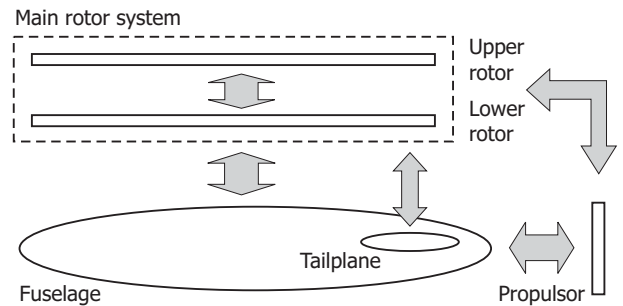


Figure 6. Schematic summarising the various aerodynamic interactions between the various components of the simulated configuration. (Interactions represented by arrows)

envelope that is associated with each rotor by plotting the trajectories of their tip vortices as they intersect the plane of lateral symmetry of the fuselage.

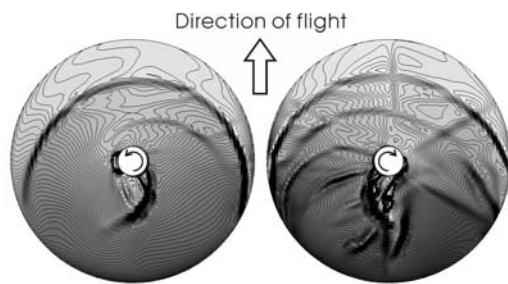
Figures 4 and 5 illustrate the complex nature of the interaction between the lifting components of the compounded coaxial helicopter and their wakes. Careful study of these images supports the notion that the aerodynamic interference between the various components of the system can be characterised in terms of two rather different possible modes of interaction. The first, rather obvious 'direct' mode involves the direct impingement of the wake of one of the components of the system on the other. The aerodynamic environment experienced by the affected component, and hence its loading, is usually modified very strongly and directly during this mode of interaction. Interaction between the wake of one of the components of the configuration and the wake of another component can result in a second 'indirect' mode of interaction, however. In this mode, the distortion of the wake of the component that is induced by the interaction usually feeds back into its aerodynamic loading in a manner that is more subtle, and often far more obscure, than during a direct interaction. Both modes of interaction have a profound influence on the aerodynamic characteristics of the helicopter configuration examined in this study.

Figure 6, adapted from the influential work of Sheridan and Smith<sup>(24)</sup>, summarises the range of interactions that are possible between the various components of the compounded coaxial system. Sheridan's network-type analysis and associated reductive approach has proved to be a very instructive means of classifying the multitude of aerodynamic interactions that can be present within the rotary-winged system and is used here to help differentiate between the various sources of aerodynamic interaction that are present within the aerodynamic environment of the compounded coaxial helicopter.

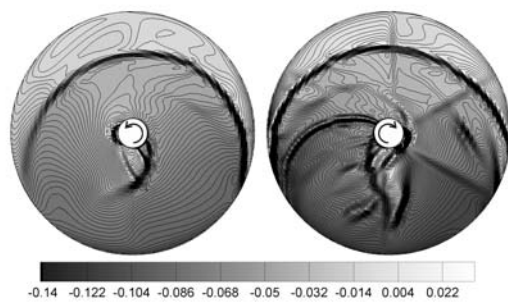
#### 5.0 MAIN COAXIAL ROTOR

The aerodynamic environment of the main rotor is strongly influenced by an indirect interaction with the fuselage that results in a significant upwards displacement of its wake. The pitching moment and download on the tailplane as a result of the direct interaction of this surface with the wake of the main rotor also feeds back through the trim conditions on the aircraft to modify very strongly the loading distribution on the main rotor system.

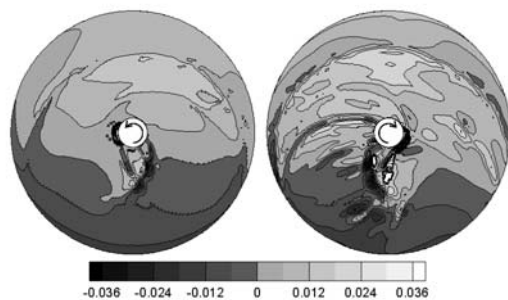
Figure 7(a) shows the distribution of inflow over the upper and lower rotors of the main rotor system of the full configuration. The inflow pattern is characterised by a strong longitudinal gradient, associated primarily with the skew, in the mean, of the vortex tube comprising the rotor wake. The distribution of inflow over the rotor discs is dissected by a series of ridges corresponding to the positions of various localised interactions between the blades of the rotors and their tip vortices. On the upper rotor, these interactions result primarily from interactions between the blades and the tip vortices



(a) Full configuration with fuselage



(b) Configuration without fuselage



(c) Difference (a) - (b)

Figure 7. Distribution of inflow,  $-v/R_c\Omega_c$ , over the main rotor discs, showing the strong interaction between the upper and lower rotors at advance ratio  $\mu = 0.15$ . (Left: upper rotor. Right: lower rotor).

from blades on the same rotor, whereas on the lower rotor a sequence of additional inter-rotor interactions are also present. Figure 7(b) shows the equivalent inflow distribution in the absence of the fuselage, and Fig. 7(c) shows the difference between the inflow through the rotor with and without the fuselage present and reveals very clearly the effect of interaction with the fuselage on the aerodynamic environment of the main rotor system. Three primary effects are apparent. Firstly, the strengths of some of the localised blade vortex interactions are modified, with the major effect being evident on the lower rotor. The shift in the pattern of localised interactions is entirely consistent with the deflection of the wake of both the upper and lower rotors that is evident in Fig. 8. In this figure, the

marked influence of the fuselage in modifying the trajectory of the vortices from the main rotor is clearly visible.

Secondly, the displacement of the free-stream by the fuselage is also responsible for a weak upflow inboard on the forward half of the lower rotor and a similar downflow on the rear of the system<sup>(25)</sup>. This dipole-like distortion to the velocity field of the rotor is particularly evident in the inflow distribution on the forward part of the lower rotor shown in Fig. 7(c); the downwash on the rear of the discs is obscured by the complex pattern of interleaving ridges that result from localised interactions between the blades and the vortices trailed from their roots. Finally, a strong difference in the longitudinal gradient of inflow is apparent when the distribution for the full configuration is compared with that of the rotors operating in isolation. This is not due primarily to the gross distortion of the wake structure alluded to earlier, but is a more direct effect of the strong nose-up pitching moment on the system that is induced by the impingement of the wake of the main rotor on the tailplane.

To expose this effect more clearly, Fig. 9 shows the associated distribution of blade loading on the upper and lower rotors of the main rotor system. The concentration of blade loading at the tips of the blades on the advancing sides of both rotors is characteristic of a very stiff coaxial rotor system. Figure 9(c), showing the difference in loading distribution on the rotors with and without the fuselage present, reveals an additional strong concentration of loading at the rear of the rotor of the full configuration. This concentration is almost entirely due to the longitudinal cyclic input that is required to produce a nose-down pitching moment to counteract the effect of the tailplane. This re-distribution of loading in order to satisfy overall trim of the aircraft has a clear impact on the power required by the main rotor system, as can be seen in Fig. 10 where a significant increase in the power consumed by the system when operated as part of the configuration rather than in isolation can be correlated with the concentration in loading at the rear of the rotor discs.

Figures 11 and 12 show the variation, over a single rotor revolution, of the thrust generated, and power consumed, by the upper and lower rotors of the main rotor system. The characteristic three-per-revolution variation of the thrust and power is a basic consequence of the aerodynamics of stiff rotor systems. The six-per-revolution variation in thrust and power that is generated predominantly by the lower rotor is an effect of the aerodynamic interference between the blades of the two rotors as they pass by each other. These interactions are also visible as the sequence of radial ridges in the inflow distributions shown in Fig. 7. Comparison of parts (a) and (b) of Figs 11 and 12 show that these vibratory characteristics of the main rotor are modified in amplitude, but not significantly in character, by integration of the rotor system into the helicopter configuration.

When installed as part of the complete helicopter configuration, however, the main rotor is required to generate sufficient additional thrust to overcome the download that it induces on the tailplane as a result of the direct impingement of its wake on this lifting surface at the advance ratio of the simulation. This increment in thrust is shared unequally between the upper and lower rotors because of the requirement that the main rotor system also maintain the aircraft in yaw equilibrium. Indeed, a comparison of Figs 11(a) and 11(b) shows the thrust required to counteract the download on the tailplane to be provided almost entirely by the upper rotor of the coaxial system.

The net effect of this interaction on the partition of thrust between the main rotor and propulsor can be inferred from Fig. 13. In the presence of the tailplane, the main rotor is required to provide a greater overall thrust to balance the download on the tailplane. A larger propulsive component to the rotor thrust thus results from the forward tilt of the main rotor. The procedure used to trim the aircraft translates this increment in propulsive force from the main rotor into a reduction in the propulsive force required from the propulsor and hence, quite surprisingly, into a fairly significant reduction in the power required by the propulsor when the rotor systems are

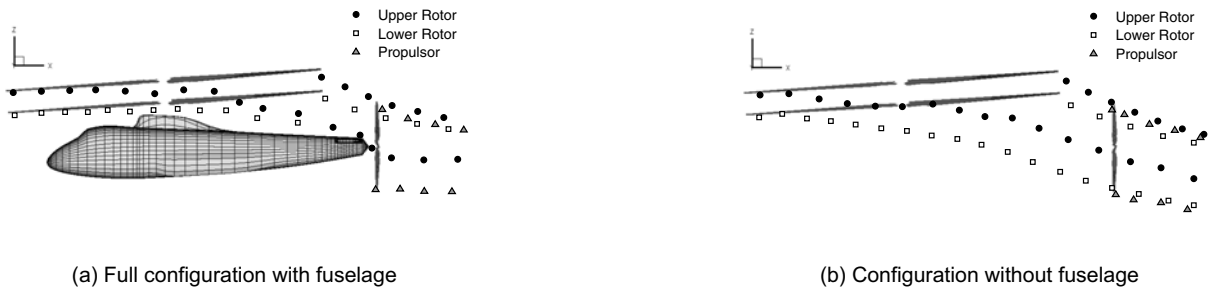


Figure 8. Trajectories of the tip vortices of the main rotors and propulsor at advance ratio  $\mu = 0.15$  showing the points of intersection of individual vortices with the longitudinal plane through the fuselage centreline at various times during a single main rotor revolution.

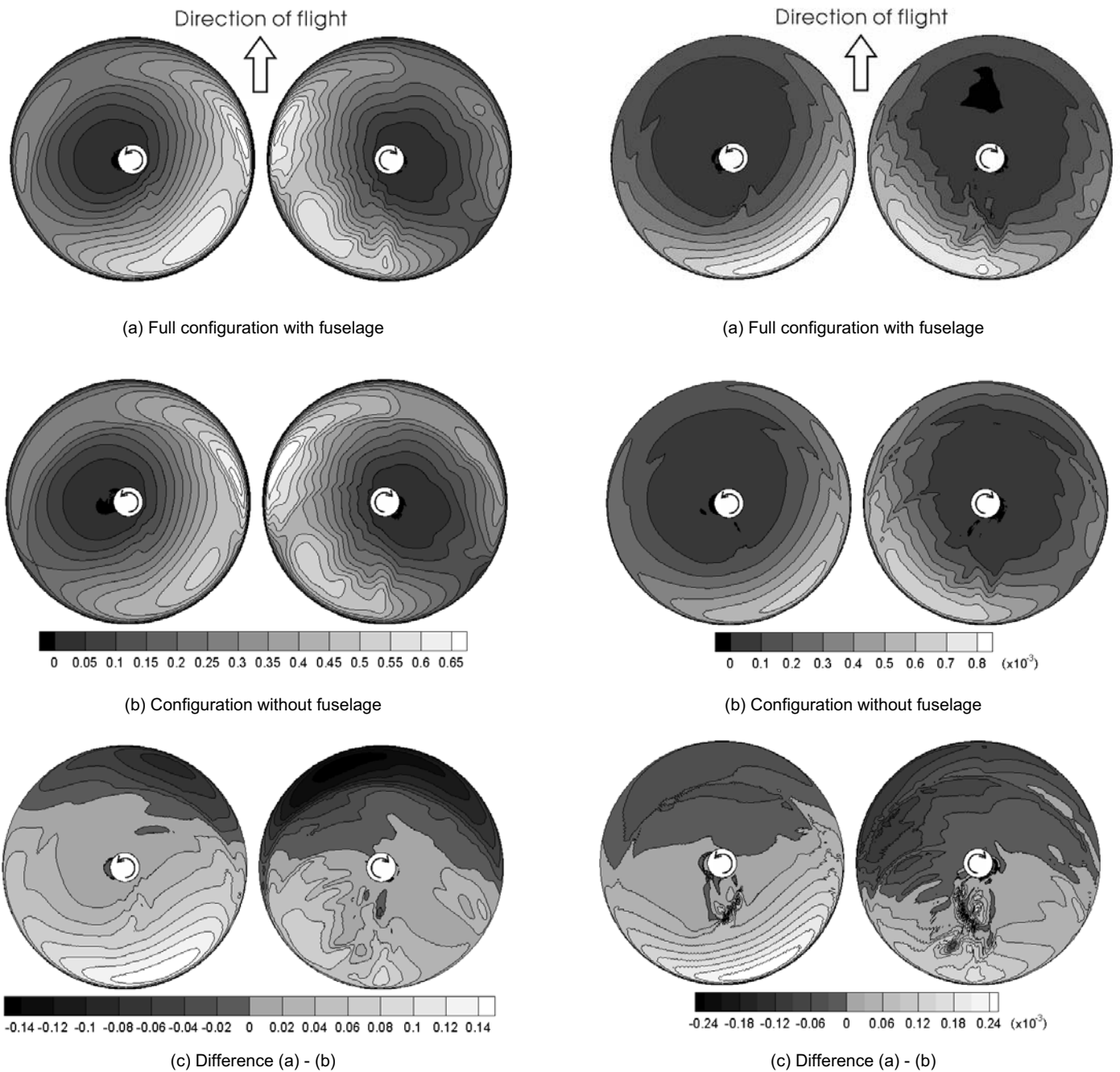
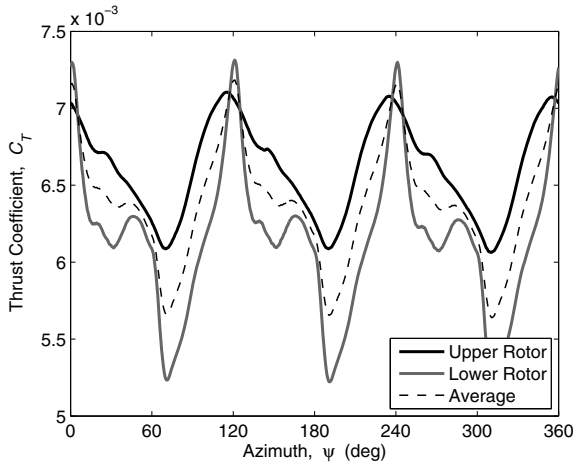
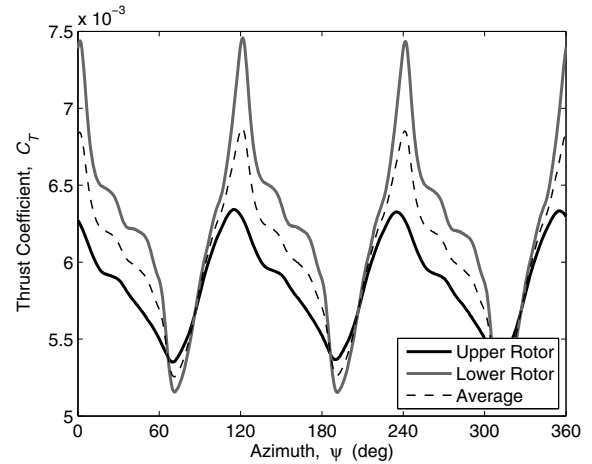


Figure 9. Distribution of blade loading over the main rotor discs at advance ratio  $\mu = 0.15$ . (Left: upper rotor. Right: lower rotor).

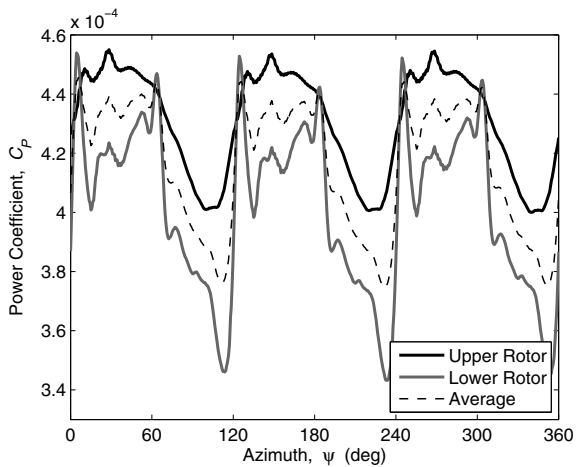
Figure 10. Distribution of power coefficient over the main rotor discs at advance ratio  $\mu = 0.15$ . (Left: upper rotor. Right: lower rotor)



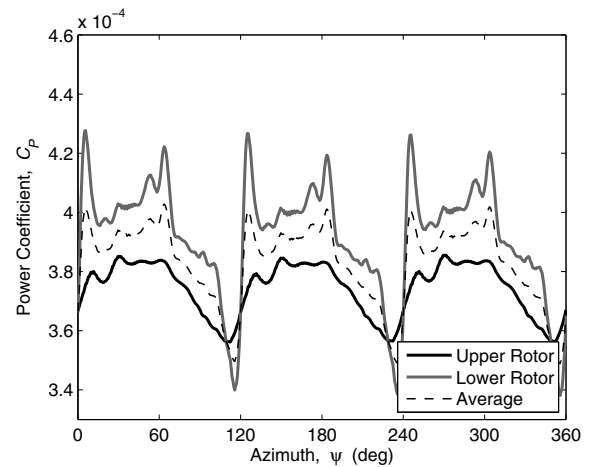
(a) Full configuration with fuselage



(b) Configuration without fuselage

Figure 11. Temporal variation in the thrust produced by the upper and lower rotors of the coaxial system over one revolution at advance ratio  $\mu = 0.15$ .

(a) Full configuration with fuselage



(b) Configuration without fuselage

Figure 12. Temporal variation in the power consumed by the upper and lower rotors of the coaxial system over one revolution at advance ratio  $\mu = 0.15$ .

integrated into the full configuration. This example illustrates the extreme care with which the scheduling of the propulsor in relation to the main rotor needs to be approached in such a configuration.

## 6.0 PROPULSOR

Figure 8 shows the very strong direct interaction that exists between the main rotor and the propulsor. The important role of the fuselage in modifying the form of this interaction is clearly evident by comparing Figs 8(a) and 8(b). With the fuselage absent, the propulsor is entirely enveloped within the main rotor wake at the advance ratio of the simulations. As shown in Fig. 8(a), the fuselage and tailplane distort the trajectories of the individual vortices from the main rotor as they are swept back into the flow behind the system. This yields a flatter, more vertically-compact wake structure that interacts with a smaller proportion of the disc area of the propulsor than when the fuselage is absent.

Figure 14 shows the effect of this interaction on the resultant structure of the wake of the propulsor itself. When operated in isolation, the propulsor generates, as expected, a steady, cylindrical,

propeller-like wake as shown in Fig. 14(a). At the advance ratio of the simulation, very little contraction of the wake is evident as it convects downstream. With the main rotor system in place, the wake of the propulsor is skewed significantly downwards due to the downwash from the main rotor, as shown in Fig. 14(b). With the fuselage present, the lower half of the wake of the propulsor is shielded from significant distortion and the wake of the propulsor adopts the rather unusual, asymmetric configuration shown in Fig. 14(c).

Figure 15 shows the distribution of loading on the propulsor disc after decomposition into mean and fluctuating (root-mean-square) components.

By comparing Figs 8 and 15, it can be seen that the locations of maximum unsteadiness in the loading on the propulsor disc correlate directly to the regions where the vortices from the main rotor pass directly through the plane of the propulsor disc. The variation in propulsive force generated by the propulsor over a single main rotor revolution is shown in Fig. 16. As expected, the loading on the isolated propulsor is entirely steady. A modulation of the propulsor thrust at the main rotor blade-passage frequency is clearly apparent when the propulsor is operated in the presence of the main rotor

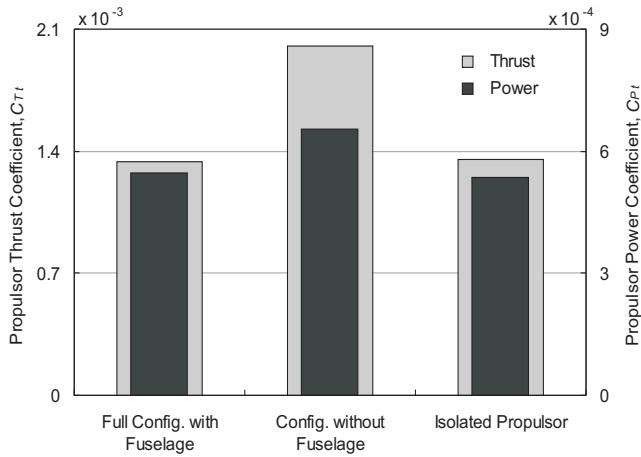


Figure 13. Comparison of the thrust generated, and power consumed, by the propulsor when operated in isolation and when operated as part of the helicopter configuration at advance ratio  $\mu = 0.15$ .

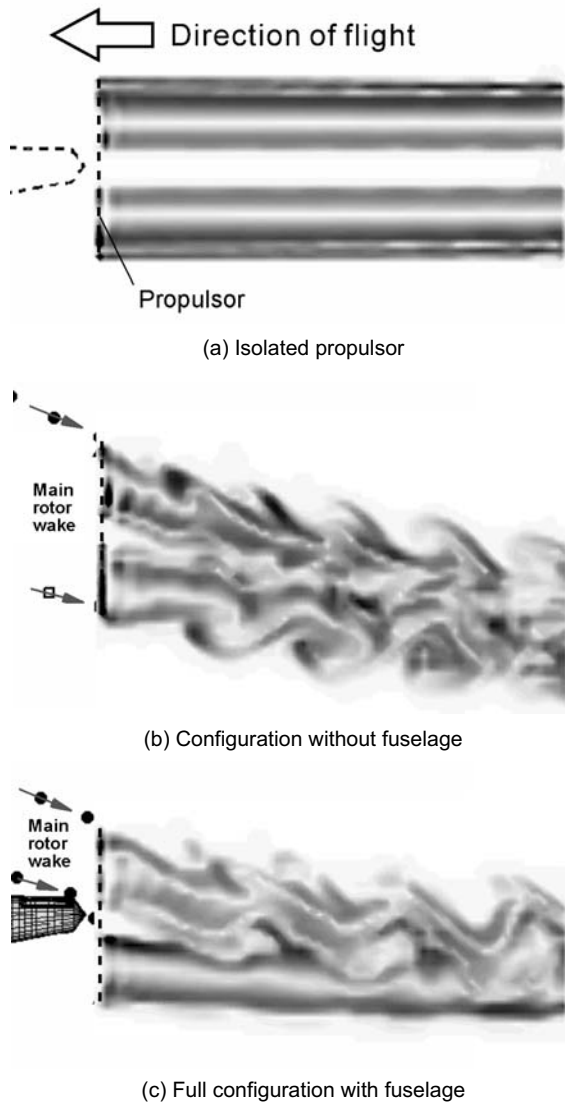


Figure 14. Comparison of propulsor wake geometry, when operated in isolation and when operated as part of the helicopter configuration at advance ratio  $\mu = 0.15$ , visualised as contours of vorticity magnitude on a vertical plane through the centreline of the fuselage

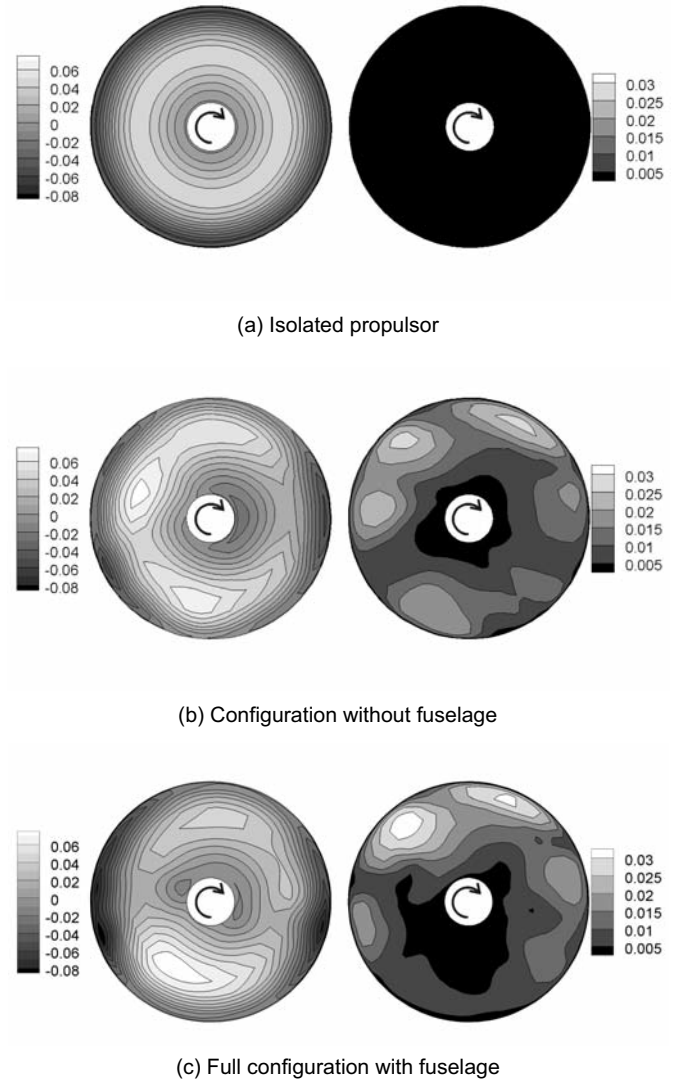


Figure 15. Distribution of blade loading coefficient over the propulsor disc, as seen from behind the helicopter at advance ratio  $\mu = 0.15$ . (Left: mean loading. Right: RMS fluctuation in loading.) Note that different scales are used for the mean and RMS loading.

system. This modulation is a direct consequence of a fairly gross variation in the aerodynamic environment of the propulsor that is caused by the fluctuating velocity field associated with the passage of the train of individual main rotor vortices through the propulsor disc. Why this modulation occurs at the main rotor blade passage frequency and not, as might be expected, at twice this frequency (given the total number of blades present on the main rotor) was explained in Ref. 5 in terms of a spatial and temporal coherence between the vortical structures that are produced in the wakes of the upper and lower rotors. This coherence results from the particular choice of phasing between the upper and lower rotors, but could quite feasibly be absent if the phasing were to be changed. A significant contribution to the unsteadiness in the loading on the propulsor at its own blade passage frequency arises only in the presence of the main rotor. This component of the unsteadiness in the loading on the propulsor is primarily an inherent characteristic of the aerodynamics of the rotor when operated in the skewed onset flow that is induced by the main rotor, but an additional contribution at blade-passage and higher frequency undoubtedly arises from smaller-scale, chopping-type interactions between the individual blades of the propulsor and the main rotor vortices.

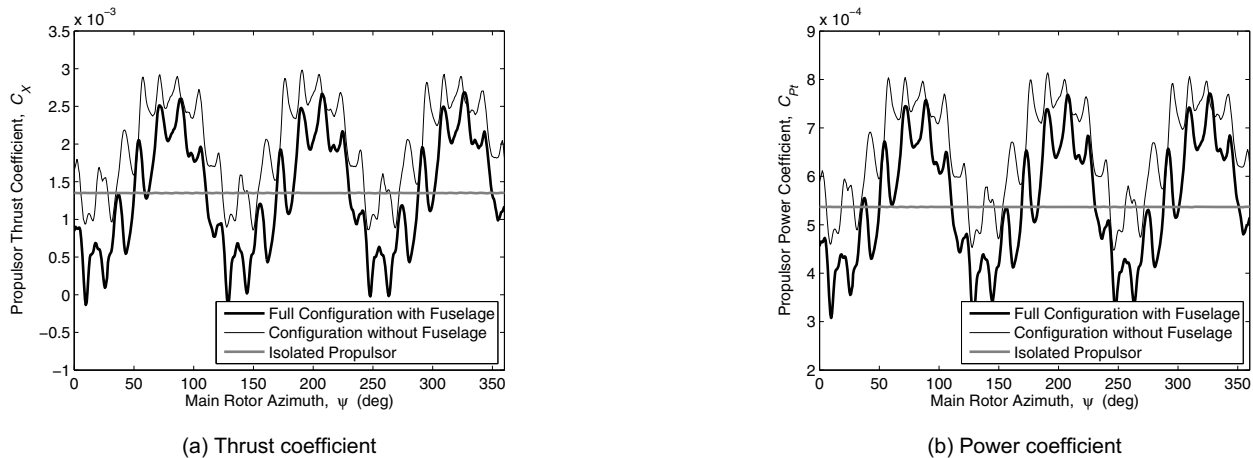


Figure 16. Temporal variation in the thrust produced and power consumed by the propulsor over one main rotor revolution at advance ratio  $\mu = 0.15$ .

## 7.0 FUSELAGE

The variation of the pressure coefficient along the top centreline of the fuselage is shown in Fig. 17. In this figure, the pressure distribution along the fuselage of the full configuration is compared with that along the isolated fuselage when flying at the same forward speed (at  $\mu = 0.15$ ). Comparing Fig. 17 with Fig. 5, it is evident that the effects of the main rotor and its wake on the mean component of pressure on the fuselage is most pronounced at the rear of the fuselage where the wake vortices pass very close to the surface of the fuselage. The limited extent of this direct interaction is a consequence of the particular advance ratio of the simulated case presented here. For similar reasons, the propulsor has minimal effect on the pressure distribution on the fuselage. At lower forward speed, where the wake of the main rotor impinges on a much larger proportion of the fuselage, the effect of the main rotor in producing a significant download on the fuselage is much more pronounced, however<sup>(5)</sup>.

The most pronounced effect of the main rotor system on the fuselage at the advance ratio of the case presented here is to introduce significant unsteadiness into the aerodynamic loading on the fuselage. The vertical bars in Fig. 17 represent the root-mean-square amplitude of the fluctuations in pressure along the top centreline of the fuselage. The greatest fluctuations are experienced

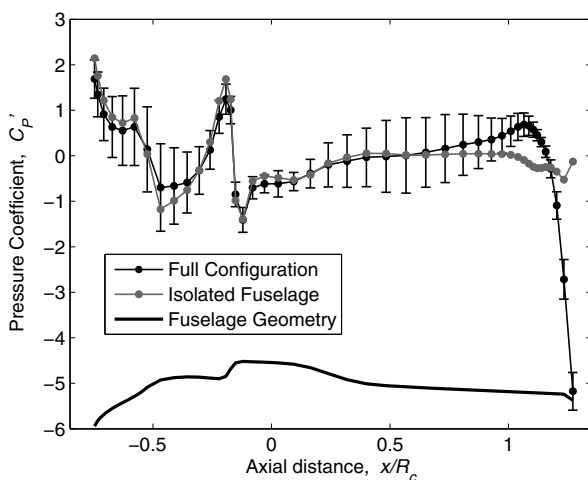


Figure 17. Pressure variation along the top centreline of the fuselage at advance ratio  $\mu = 0.15$ . (Mean signal represented by curves, root-mean-square amplitude of fluctuating signal represented by error bars)

on those parts of the fuselage that lie directly below the main rotor blades. To reveal the origins of the pressure fluctuations in more detail, Fig. 18 shows the pressure along the top centreline of the fuselage, plotted as a function of main rotor azimuth (in other words, as a function of time). The plot shows two distinct types of feature. The most obvious features in this diagram are the horizontal ridges of elevated pressure that extend from the nose of the helicopter to just short of the hub of the main rotor (at  $x/R_c = 0$ ), then continue, after a short time delay, from just aft of the main rotor hub to near the tail. The form of these features is indicative of a series of disturbances that are felt instantaneously along a significant proportion of the fuselage. The three-per-revolution character of these features, and their phasing between the front and rear of the fuselage, reveals them to be caused by the direct passage over the fuselage of the blades of the main rotor. The three-per-revolution rather than six-per-revolution character of these disturbances is again a consequence of the rotor phasing – the upper and lower rotors of the simulated configuration were arranged to overlap with the blades aligned with the longitudinal axis of the fuselage. It appears that with this particular choice of phasing the disturbances from the upper and lower rotors combine to yield the strongest effect on the unsteady loading on the fuselage. The amplitude of these blade overpressure-type events could quite feasibly be altered though by modifying the phasing of the upper and lower rotors, but not without consequence

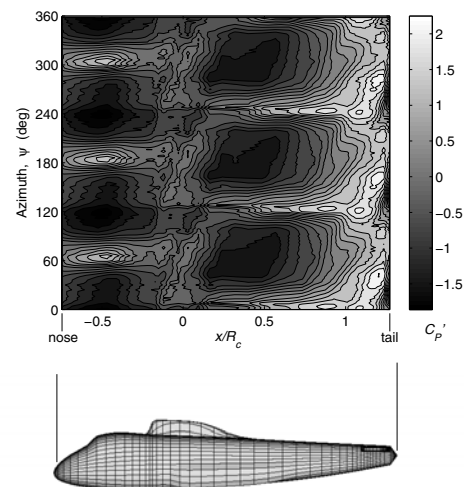
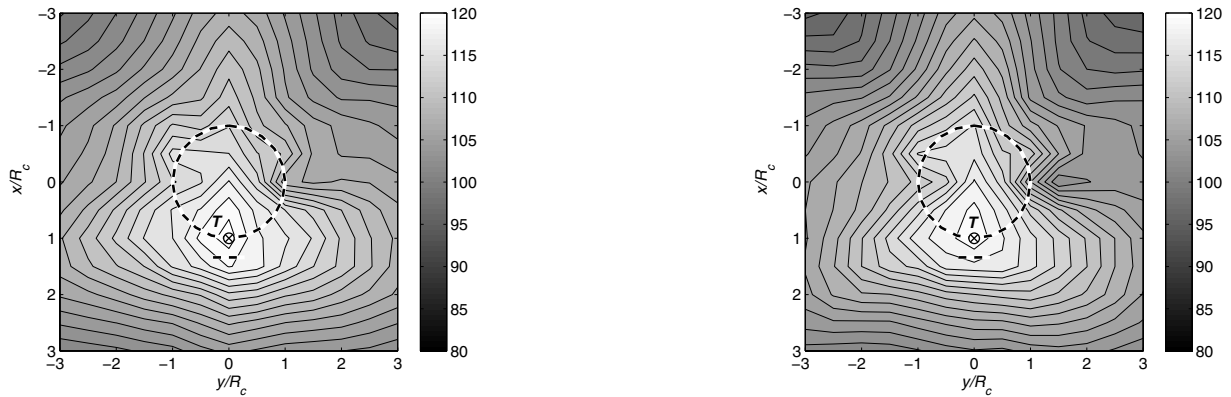


Figure 18. Pressure distribution along the top centreline of the fuselage as a function of time (main rotor azimuth) at advance ratio  $\mu = 0.15$ . Mean component of signal removed.



(a) Full configuration with fuselage (sound pressure at 'T' is 120.7dB)

(b) Configuration without fuselage (sound pressure at 'T' is 114.7dB)

Figure 19. Overall sound pressure level (in decibels) produced by the main rotor and propulsor on a plane parallel to the ground, one rotor radius below the hub of the lower main rotor at advance ratio  $\mu = 0.15$ . (Rotor positions marked by dashed lines)

for the unsteadiness in the loading on the propulsor alluded to earlier, and possibly also for the acoustic signature of the system as described later in this paper.

The secondary, diagonal features in this form of presentation of pressure data are characteristic of pressure disturbances that are induced by the convection along the length of the fuselage of vortical structures within the flow. Comparison of Figs 4(b) and 18 shows these disturbances to be associated primarily with the passage of the root vortices (for  $-0.1 < x/R_c < 0.3$ ) and the tip vortices (for  $1.0 < x/R_c < 1.3$ ) from the main rotor in close proximity to the surface of the fuselage.

## 8.0 INTERACTIONAL AEROACOUSTICS

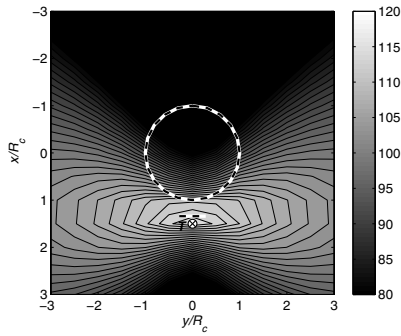
This final section of the paper considers the effect of the aerodynamic interactions between the various components of the system on the noise produced by the thrust-compounded hingeless coaxial configuration. The radiated acoustic field of the vehicle is computed using the Farassat-1A formulation of the Ffowcs Williams-Hawking equations<sup>(26)</sup>. In the present numerical implementation, the aerodynamic force contributed by each blade panel is used to construct a point acoustic source at the centre of each panel. The sound that is radiated by each of these sources is then integrated to represent the loading noise that is produced by the blades. The aerodynamic model assumes an infinitesimally thin blade; the thickness noise has thus to be modelled independently. This is done by attaching a source-sink pair to each blade panel. Noise due to quadrupole terms is neglected in the present work as is any acoustic radiation or reflection from the fuselage. The same methodology has previously yielded good predictions of the acoustic characteristics of the rotor used in the HART II series of experiments<sup>(27)</sup>. In the interests of brevity, data for only one observer plane, located one rotor radius below the hub of the lower main rotor, is presented here. The acoustic sources are scaled to represent the noise that is generated by an aircraft with a main rotor radius of 5.5m, a main rotor speed of 345rpm and an all-up weight of 5,562kg and thus to be representative of a helicopter of the size and weight of the XH-59A<sup>(16)</sup>.

Figure 19 shows contours of overall sound pressure on the observer plane below the helicopter, and reveals the very large contribution to the noise produced by the system on this plane from the propulsor. The thickness noise produced by the propulsor is particularly significant<sup>†</sup> because of the rotor's relatively high tip Mach number ( $M = 0.7$  assuming sea-level conditions). Figure 20(a) shows the contribution to the noise on the observer plane from the propulsor in isolation, and illustrates how its noise radiates directly outwards within its tip-path plane to produce a narrow band of

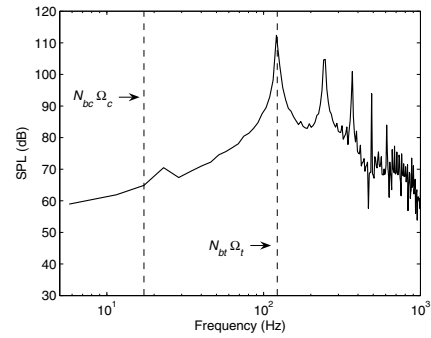
extremely high acoustic pressure on the observer plane. The maximum sound pressure level produced by the propulsor on the observer plane is estimated to be approximately 115dB. It should be noted though that the design of the blades of the simulated propulsor is exceptionally simple and that, in practice, the acoustic signature of this device could quite feasibly be ameliorated by the introduction of tip sweep or by more appropriate aerofoil selection. As shown in Fig. 20(b), the noise from the propulsor, as might be expected from the observations made above, is concentrated at its blade passage frequency and integer multiples thereof<sup>f(28)</sup>. When integrated into the full configuration, the noise produced by the propulsor on the observer plane is distorted quite significantly by the loading perturbations that are induced by its interaction with the main rotor. Comparing Figs 20 and 21, it can be seen that these aerodynamic interactions cause a significant proportion of the acoustic radiation from the propulsor to be directed forward along the longitudinal axis of the aircraft.

The aerodynamic interactions within the system also have a significant effect on the noise that is produced by the main rotor. Figure 22 shows the contribution of the main rotor system to the sound pressure level on the observer plane below the helicopter. In the absence of the aerodynamic influence of the fuselage, the position of maximum sound intensity (marked 'T' in the diagram) is located significantly further forward below the rotor in comparison to its position on the full configuration. This is consistent with the shift in loading on the rotor, described earlier, that is required to trim the pitching moment on the aircraft that is induced by the impingement of the wake of the main rotor on the tailplane. The maximum sound pressure produced by the main rotor is about 119dB, and is about 1dB higher for the full configuration than when the fuselage is absent. Figure 23 shows the same data as presented in Fig. 22, filtered to contain only those harmonics between 5 to 40 times the main rotor blade-passage frequency and hence to expose the component of noise that can be associated directly with the blade vortex interactions (BVIs) that are responsible for the well-defined, ridge-like perturbations in the inflow distribution through the main rotor shown in Fig. 7. In Ref. 5 it was surmised that the concentration in loading on the rear of the disc in response to the requirement to trim the moment from the tailplane was the primary reason for the concentration of BVI-related sound below the left rear of the main rotor system. Comparison of Figs 23(a) and 23(b), which contrast the BVI-related acoustic signature of the aircraft with and without the tailplane (and fuselage) present, shows the extent of the region of maximum BVI sound intensity to be quite significantly altered in the presence of the fuselage and hence supports this interpretation. A change in maximum BVI-related sound pressure at the location of maximum sound pressure level (marked 'B' in the

<sup>†</sup> It appears that this thickness contribution to the propulsor noise was significantly underestimated in the work of Kim *et al*<sup>(5)</sup>.

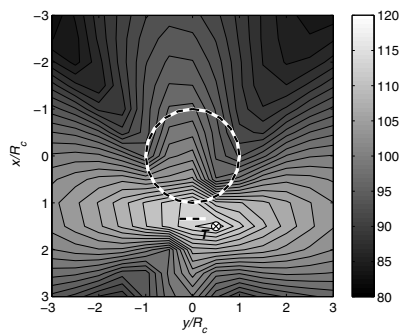


(a) Total noise produced by the propulsor (sound pressure at 'T' is 114.9dB)

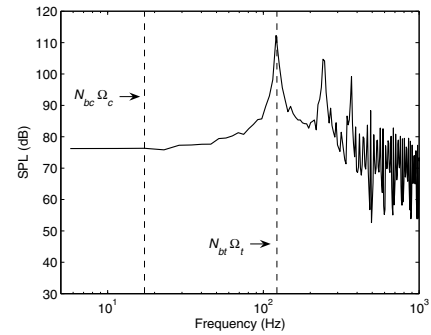


(b) Frequency spectrum of acoustic pressure at point 'T' in figure at left

Figure 20. Overall sound pressure level (in decibels) produced by the propulsor on a plane parallel to the ground, one rotor radius below the hub of the lower main rotor when operated in isolation at advance ratio  $\mu = 0.15$ . (Rotor positions marked by dashed lines.)

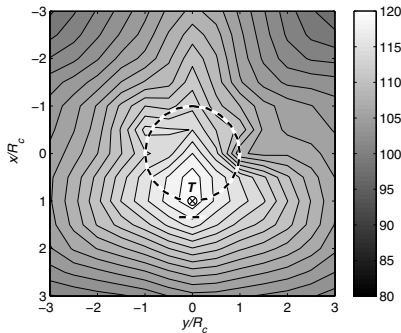


(a) Total noise produced by the propulsor (sound pressure at 'T' is 114.7dB)

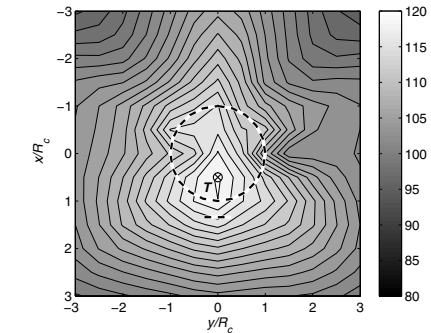


(b) Frequency spectrum of acoustic pressure at point 'T' in figure at left

Figure 21. Contribution from the propulsor to the sound pressure level (in decibels) produced by the full helicopter configuration on a plane parallel to the ground, one rotor radius below the hub of the lower main rotor at advance ratio  $\mu = 0.15$ . (Rotor positions marked by dashed lines.)

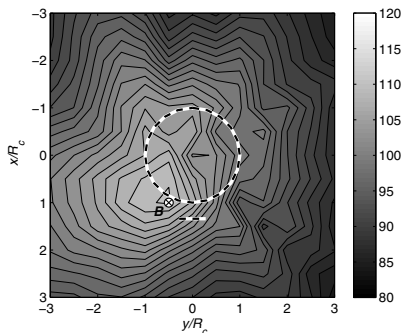


(a) Full configuration with fuselage (sound pressure at 'T' is 119.7dB)

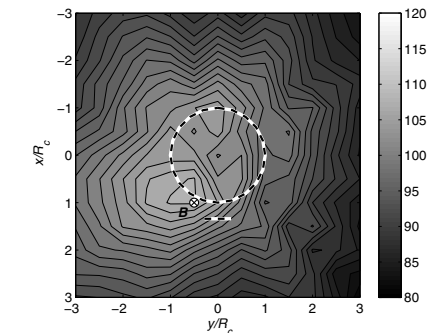


(b) Configuration without fuselage (sound pressure at 'T' is 119.0dB)

Figure 22. Contribution from the main rotor to the sound pressure level (in decibels) produced by the helicopter configuration on a plane parallel to the ground, one rotor radius below the hub of the lower main rotor at advance ratio  $\mu = 0.15$ . (Rotor positions marked by dashed lines.)



(a) Full configuration with fuselage (sound pressure at 'B' is 110.2dB)



(b) Configuration without fuselage (sound pressure at 'B' is 107.7dB)

Figure 23. Contribution from the main rotor to the sound pressure level (in decibels) in the BVI frequency range produced by the helicopter configuration on a plane parallel to the ground, one rotor radius below the hub of the lower main rotor at advance ratio  $\mu = 0.15$ . (Rotor positions marked by dashed lines.)

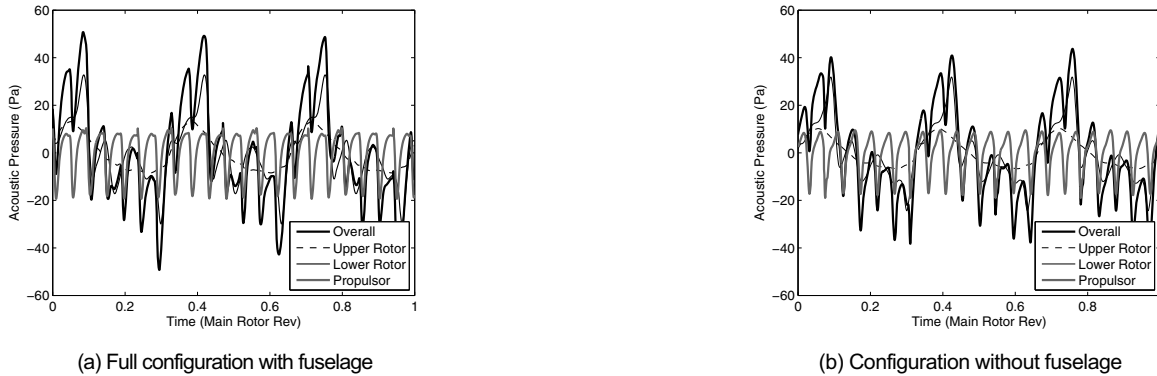


Figure 24. Time-history of acoustic pressure at the locations of maximum sound pressure level, marked 'T' in Fig. 19.

diagrams) from 108dB with the fuselage absent to about 110dB for the full configuration is most likely a response to the subtle changes in the strength and position of individual BVIs that was referred to in connection with Fig. 7 and that was attributed to the distortion of the trajectory of the wake of the main rotor by the fuselage.

The strong influence of the propulsor runs the risk of obscuring the rather subtle effect of the interactions within the system on the acoustic signature of the entire aircraft. It should be borne in mind that the acoustic influence of the propulsor is spatially rather confined, and indeed, away from the disc-plane of the propulsor, the acoustic signature of the vehicle consists of a more balanced combination of acoustic contributions from the propulsor and main rotor. Figure 24, for instance, shows the history, over a single main rotor revolution, of the acoustic pressure at the points marked 'T' in the plots of overall sound pressure level on the observer plane below the helicopter shown in Fig. 19. This figure reveals the rather different character of the acoustic contribution from the upper and lower rotors of the coaxial system – the contribution from the upper rotor is essentially at its blade-passage frequency and lacks the higher-harmonic content that arises on the lower rotor as a result of its loading being more strongly influenced by localised blade vortex interactions. At this observer location, the acoustic contribution from the propulsor is primarily at its blade passage frequency, but has a clearly observable, additional component that appears to be aperiodic and that arises from its interaction with the wake from the main rotor. The influence of the interaction between the main rotor, fuselage and tailplane, through the mechanisms described earlier, in increasing the peak-to-peak acoustic signal from the system by approximately 10Pa (which translates to about 6dB difference) is also more clearly apparent in this rendition of the data than perhaps in the maps of overall sound pressure level presented above.

## 9.0 CONCLUSION

The aerodynamics and acoustics of a generic coaxial helicopter with a stiff main rotor system and a tail-mounted propulsor have been investigated using Brown's Vorticity Transport Model. By comparing the aerodynamics of the full configuration of the helicopter to the aerodynamics of various combinations of its sub-components, the influence of the various aerodynamic interactions within the system on its behaviour can be isolated.

The traditional approach to the analysis of interactional effects on the performance of the helicopter relies on an initial characterisation of the system in terms of a network of possible interactions between the separate components of its configuration. Thus, within the configuration under study, it is possible to identify the effect of the main rotor on the fuselage and propulsor, the distortion of the

wake of the main rotor that is caused by the presence of the fuselage and so on. The characteristics of these various interactions and their effects on the performance of the system have been described in detail within this paper.

Many of the interactions that have been exposed within the aerodynamics of the configuration presented here do exhibit a relatively linear relationship between cause and effect and hence are amenable to a reductionist approach such as this. For instance, the distortion of the wake of the main rotor by the fuselage has a marked effect on the loading generated by the propulsor, but the effect on the propulsor is prevented from feeding back into the performance of the main rotor. This is because of the isolation that is provided by the particular method that is used to trim the vehicle, and also by the inherent directionality of the interaction that results from its physics being dominated by the convection of the wakes of the two systems into the flow behind the vehicle.

Several of the interactions that have been observed for this helicopter configuration exhibit a less direct relationship between cause and effect, however. These interactions are characterised by strong feedback or closed-loop type behaviour, in certain cases through a path which remains relatively obscure and hidden within the network of interactions that form the basis of the traditional reductionist type approach. For instance, the load that is induced on the tailplane by the direct impingement of the wake of the main rotor requires, through the requirement for overall trim of the forces and moments on the aircraft, a compensatory change in the loading distribution on the main rotor itself, which then modifies the strength of its wake and hence in circular fashion, the loading on the tailplane itself. Without this understanding of the strong mutual coupling between the performance of the tailplane and the main rotor, the observed dependence of the acoustic radiation of the aircraft on the presence or not of the tailplane (or, in practical terms, more likely on its design and positioning) may appear to the analyst as a very obscure and possibly even unfathomable interdependence within the system.

Thus, although the reductionist, network-based approach to classifying the interactions present within the system is conceptually appealing and simple, it must be realised that the possible presence of feedback loops deep within the interactional aerodynamics, such as the one described above, may cause the approach to miss, obscure or hide the presence of interactions between some of the various sub-components of the system. The analysis presented in this paper warns against an overly literal application of this reductive, building-block type approach to the categorisation of the interactions that are present within the system. Going further, the analysis presented in this paper suggests quite strongly that there may be no real substitute for detailed simulations of the entire configuration if the effects on the performance of the vehicle of the most deeply hidden interactions within the system are to be exposed. The results presented here show that modern simulations

are indeed capable of representing the very wide range of aerodynamic interactions that are present within the helicopter system, even one as complex as the compounded coaxial system studied in this paper. This bodes well for the assertion that modern computational techniques may be in a position to help forestall future repetition of the long history of unforeseen, interaction-induced dynamic problems that have arisen during the development from prototype to production of many new helicopter designs.

## DEDICATION

The authors would like to dedicate this paper to the memory of Mr Ki Youn Kim (1932-2008), with grateful thanks from author HWK for the care and support that Mr Kim has provided him during the course of his PhD studies.

## REFERENCES

- BAGAL, A. Aerodynamic Design of the Sikorsky X2 Technology Demonstrator™ Main Rotor Blade, American Helicopter Society 64<sup>th</sup> Annual Forum, 29 April-1 May 2008, Montréal, Canada.
- BURGESS, R.K. The ABC™ Rotor – A Historical Perspective, American Helicopter Society 60th Annual Forum, 7-10 June 2004, Baltimore, MD, USA.
- LINDEN, A.W. and RUDDLELL, A.J. An ABC Status Report, American Helicopter Society 37th Annual Forum, 17-20 May 1981, New Orleans, LA, USA.
- ORCHARD, M. and NEWMAN, S. The fundamental configuration and design of the compound helicopter, Proceedings of Institution of Mechanical Engineers, **217** Part G: *J Aerospace Engineering*, G01702, October 2003, pp 297-315.
- KIM, H.W., KENYON, A.R., DURAISAMY, K. and BROWN, R.E. Interactional aerodynamics and acoustics of a propeller-augmented compound coaxial helicopter, American Helicopter Society Aeromechanics Specialists' Meeting, 23-25 January 2008, San Francisco, CA, USA.
- BROWN, R.E. Rotor wake modeling for flight dynamic simulation of helicopters, *AIAA J*, January 2000, **38**, (1), pp 57-63.
- BROWN, R.E. and LINE, A.J. Efficient high-resolution wake modeling using the vorticity transport equation, *AIAA J*, April 2005, **43**, (7), pp 1434-1443.
- KENYON, A.R. and BROWN, R.E. Wake dynamics and rotor-fuselage aerodynamic interactions, American Helicopter Society 63rd Annual Forum, 1-3 May 2007, Virginia Beach, VA, USA.
- KIM, H.W. and BROWN, R.E. Coaxial rotor performance and wake dynamics in steady and manoeuvring flight, American Helicopter Society 62nd Annual Forum, 9-11 May 2006, Phoenix, AZ, USA.
- FELKER III, F.F. Performance and loads data from a wind tunnel test of a full-scale, coaxial, hingeless rotor helicopter, NASA TM 81329/USAARADCOM TR 81-A-27, October 1981.
- KIM, H.W. and BROWN, R.E. Impact of trim strategy and rotor stiffness on coaxial rotor performance, 1st AHS/KSASS International Forum on Rotorcraft Multidisciplinary Technology, 15-17 October 2007, Seoul, Korea.
- RUDDLELL, A.J. Advancing Blade Concept (ABC™) Development, American Helicopter Society 32nd Annual Forum, 10-12 May 1976, Washington, DC, USA.
- BURGESS, R.K. Development of the ABC Rotor, American Helicopter Society 27th Annual Forum, May 1971, Washington, DC, USA.
- COOPER, D.E. YUH-60A Stability and control, *J American Helicopter Society*, 1978, **23**, (3), pp 2-9.
- PROUTY, R.W. and AMER, K.B. The YAH-64 Empennage and tail rotor – A technical history, American Helicopter Society 38th Annual Forum Proceedings, Anaheim, CA, USA, 4-7 May 1982, pp 247-261.
- MAIN, B.J. and MUSSI, F. EH101 – Development Status Report, Proceedings of the 16th European Rotorcraft Forum, Glasgow, UK, 18-20 September 1990, pp III.2.1.1-12.
- CASSIER, A., WENECKERS, R. and POURADIER, J. Aerodynamic development of the Tiger helicopter, proceedings of the American Helicopter Society 50th Annual Forum, 11-13 May 1994, Washington DC, USA.
- EGLIN, P. Aerodynamic design of the NH90 helicopter stabilizer, Proceedings of the 23rd European Rotorcraft Forum, 16-18 September 1997, Dresden, Germany, pp 68.1-10.
- FREDERICKSON, K.C. and LAMB, J.R. Experimental investigation of main rotor wake induced empennage vibratory airloads for the RAH-66 Comanche helicopter, Proceedings of the American Helicopter Society 49th Annual Forum, 19-21 May 1993, St Louis, MO, USA, pp 1029-1039.
- DINGELDEIN, R.C. Wind-tunnel studies of the performance of multi-rotor configurations, NACA TN-3236, August 1954.
- PAGLINO, V.M. and BENO, E.A. Full-scale wind-tunnel investigation of the advancing blade concept rotor system, USAAMRDL TR 71-25, August 1971.
- HALLEY, D.H. ABC helicopter stability, control, and vibration evaluation on the Princeton dynamic model track, American Helicopter Society 29th Annual Forum, Washington, DC, USA, May 1973.
- PAGLINO, V.M. Forward flight performance of a coaxial rigid rotor, American Helicopter Society 27th Annual Forum, May 1971, Washington, D.C., USA.
- SHERIDAN, P.F. and SMITH, R.P. Interactional Aerodynamics – A New Challenge to Helicopter technology, *J American Helicopter Society*, January 1980, **25**, (1), pp 3-21.
- LEISHMAN, J.G. *Principles of Helicopter Aerodynamics*, 2nd Ed, 2006, Cambridge University Press, Cambridge, UK.
- FARASSAT, F. and SUCCI, G.P. A review of propeller discrete frequency noise prediction technology with emphasis on two current methods for time domain calculations, *J Sound and Vibration*, 1980, **71**, (3), pp 399-419.
- KELLY, M.E., DURAISAMY, K. and BROWN, R.E. Blade vortex interaction and airload prediction using the vorticity transport model, American Helicopter Society Specialists' Conference on Aeromechanics, San Francisco, CA, USA, 23-25 January 2008.
- MAGLIOZZI, B., HANSON, D.B. and AMIET, R.K. Aeroacoustics of Flight Vehicles: Theory and Practice, NASA, USA.